

X-ray and Radio Studies of the candidate Millisecond Pulsar Binary 4FGL J0935.3+0901

Dong Zheng¹, Zhong-Xiang Wang^{1,2,3}, Yi Xing³ and Jithesh Vadakkumthani^{4,5}

¹ Department of Astronomy, School of Physics and Astronomy, Yunnan University, Kunming 650091, China

² Key Laboratory of Astroparticle Physics of Yunnan Province, Yunnan University, Kunming 650091, China *wangzx20@ynu.edu.cn*

³ Shanghai Astronomical Observatory, Chinese Academy of Sciences, 80 Nandan Road, Shanghai 200030, China

⁴ Inter-University Centre for Astronomy and Astrophysics, PB No.4, Ganeshkhind, Pune-411007, India

⁵ Department of Physics, University of Calicut, Malappuram-673635, Kerala, India

Received 20xx month day; accepted 20xx month day

Abstract 4FGL J0935.5+0901, a γ -ray source recently identified as a candidate redback-type millisecond pulsar binary (MSP), shows an interesting feature of having double-peaked emission lines in its optical spectrum. The feature would further suggest the source as a transitional MSP system in the sub-luminous disk state. We have observed the source with *XMM-Newton* and Five-hundred-meter Aperture Spherical radio Telescope (FAST) at X-ray and radio frequencies respectively for further studies. From the X-ray observation, a bimodal count-rate distribution, which is a distinctive feature of the transitional MSP systems, is not detected, while the properties of X-ray variability and power-law spectrum are determined for the source. These results help establish the consistency of it being a redback in the radio pulsar state. However no radio pulsation signals are found in the FAST observation, resulting an upper limit on the flux density of $\sim 4 \mu\text{Jy}$. Implications of these results are discussed.

Key words: stars: pulsars — binaries: close — gamma rays:stars

1 INTRODUCTION

Millisecond pulsars (MSPs) form from low-mass X-ray binaries (LMXBs), in which a neutron star gains angular momentum by accreting mass that is transferred from a Roche-lobe filling companion star

(Bhattacharya & van den Heuvel 1991). As one type of the end products of binary evolution, a class of so-called ‘redback’ MSP binaries has recently been recognized (Roberts 2013) and gained attention. These close MSP binaries contain a $\geq 0.1M_{\odot}$ companion star, constituting a class sample that helps reveal not only the LMXB evolution processes (Chen et al. 2013; Benvenuto et al. 2014) but also intriguing physical properties of compact star binaries (Strader et al. 2019 and references therein). Moreover, two of redbacks (PSR J1023+0038 and XSS J12270–4859; Archibald et al. 2009; Bassa et al. 2014) have been identified as transitional MSP (tMSP) systems and several as candidates (e.g., Miller et al. 2020 and references therein): these systems can switch between the states of having an accretion disk (a so-called sub-luminous disk state) and being a disk-free, rotation-powered radio binary pulsar. Interesting multi-wavelength properties have been seen in the tMSPs; for details, see, e.g., Patruno et al. (2014); Stappers et al. (2014); Takata et al. (2014); Shahbaz et al. (2015); Miller et al. (2020). Generally when in the disk state, no radio pulsed emission is detectable; while in the disk-free state, tMSPs appear like regular redbacks.

The all-sky survey capability of the Large Area Telescope (LAT) onboard *the Fermi Gamma-ray Space Telescope (Fermi)* has greatly enabled the identification of redbacks. Candidate MSPs including redbacks can be selected from unidentified sources detected by *Fermi* LAT, and followup multi-wavelength observations will allow identification of redbacks by comparing obtained properties to those of the known systems. Of course, detection of millisecond pulsations and orbitally periodic variations is required in order to identify a redback (otherwise a source would be considered as a candidate). Recently we have identified a candidate redback using the approach, for which the source in the *Fermi* LAT fourth source catalog (4FGL; Abdollahi et al. 2020), 4FGL J0935.3+0901, was targeted and a 2.5-h binary was found (Wang et al. 2020). Considering the observational facts, the source’s γ -ray variability and curved spectrum, a faint X-ray counterpart (to the binary), and double-peaked optical emission lines (H_{α} , H_{β} , and He I) of the binary (likely indicating the presence of a $\sim 10^{10}$ cm size accretion disk), we have suggested 4FGL J0935.3+0901 as a candidate redback and also likely a transitional system in the sub-luminous disk state.

The tMSPs in the disk state have distinctive properties. One is their bimodal count-rate distributions at X-rays (Patruno et al. 2014; Bogdanov & Halpern 2015; Coti Zelati et al. 2019; Miller et al. 2020). Between two distinguishable count-rate levels, a tMSP would switch quickly. Whether 4FGL J0935.3+0901 has this property can be checked with a targeted X-ray observation. The ratios of 0.5–10 keV X-ray fluxes to 0.1–100 GeV γ -ray ones for the tMSPs and candidates are ~ 0.3 – 0.4 , significantly higher than those of redbacks (e.g., Miller et al. 2020), but the previously estimated flux ratio for 4FGL J0935.3+0901 (at 0.3–10 keV X-ray band) was only ~ 0.02 . This inconsistency thus raises a question about the nature of 4FGL J0935.3+0901 and also about how to explain its double-peaked emission line feature. In addition to being the indicator of an accretion disk, the other possibility that the emission feature might reflect the intrabinary interaction processes was discussed in Wang et al. (2020). The latter possibility would suggest the source as a regular redback, and then a pulsar’s pulsed emission might be detectable (note that there are candidate redbacks in which radio pulsars are not detected; see, e.g., Strader et al. 2019). A deep radio observation may clarify the nature of the source.

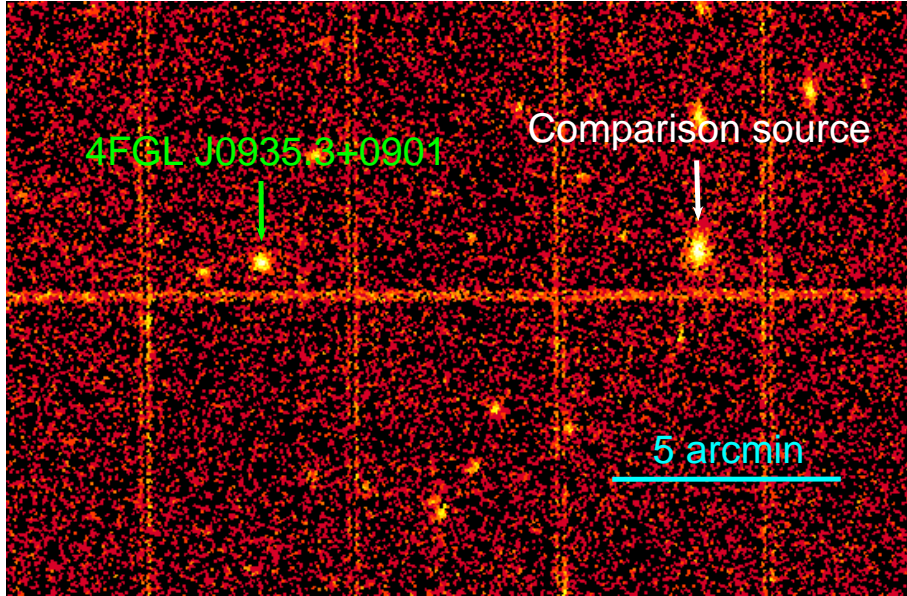


Fig. 1: *XMM-Newton* pn image of the source field, with J0935.3+0901 and a comparison source indicated.

In order to further study this source, understanding its properties and identifying its nature, we applied for *XMM-Newton* and Five-hundred-meter Aperture Spherical radio Telescope (FAST) times for X-ray and radio observations of the source respectively. In this paper, we report the results from the observations.

2 OBSERVATIONS AND DATA ANALYSIS

2.1 *XMM-Newton* Observation

We observed 4FGL J0935.3+0901 on 2020 November 12 with the European Photon Imaging Camera (EPIC) onboard the *XMM-Newton* space telescope. The total on-source observing time was $\simeq 10.7$ ks. The observation (ObsID 0860350101) was conducted in the full-frame mode with the thin optical filter used. The data were processed with the Science Analysis Software (SAS) data reduction package (version 18.0.0). Full-field background light curves in 10–12 keV were extracted for the purpose of checking any presence of particle flares in the pn and MOS1/MOS2 data. No background flares were seen in our data.

J0935.3+0901 was detected at the position of R.A.= $09^h35^m20^s.9$, Decl.= $09^\circ00'38''.27$, with a 1σ uncertainty of $0''.50$ (the 1σ systematic uncertainty for the position is $1''.5$). The source was faint, with flux approximately equal to that estimated from the *Neil Gehrels Swift Observatory* (*Swift*) detection (Wang et al. 2020). In order to study its X-ray variability, we chose a source detected in the field as a comparison source. This source, at R.A.= $09^h34^m44^s.9$ and Decl.= $09^\circ03'54''.72$ (with a 1σ uncertainty of $0''.40$), was only slightly brighter than our target. We note that this source could be a quasar based on its power-law spectrum (photon index $\Gamma \simeq 2.57$) and the comparison of its optical and X-ray fluxes ($V \simeq 18.8$ and unabsorbed flux $\simeq 2.8 \times 10^{-13}$ erg s $^{-1}$ cm $^{-2}$, respectively; see, e.g., He et al. 2019). However we still used this source because other sources in the field were too faint and no significant variability was seen in our following analysis of this comparison source.

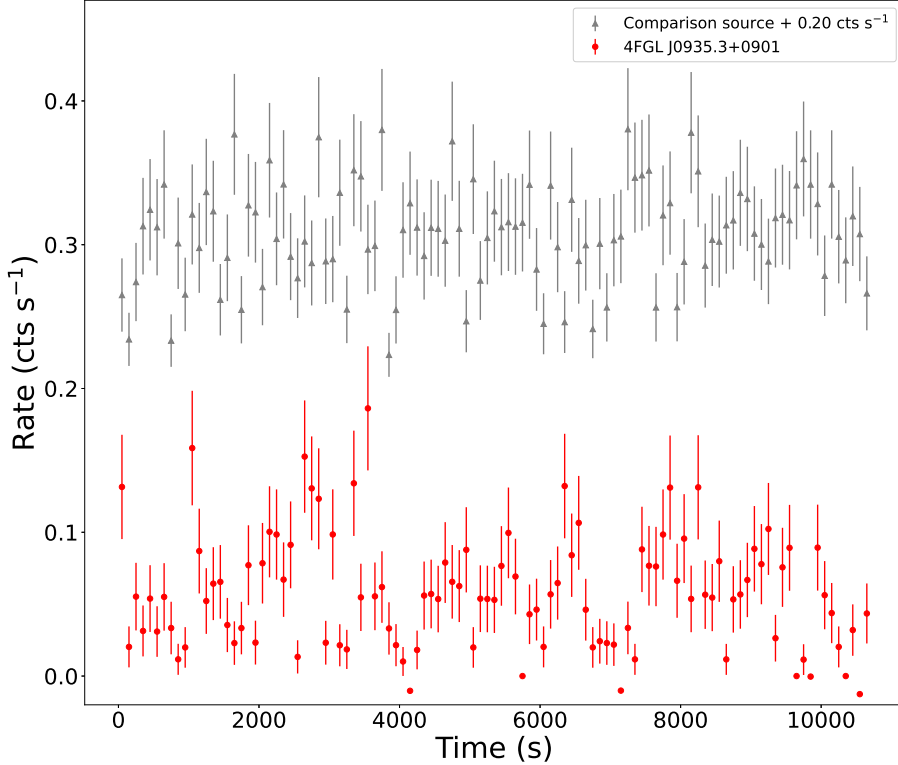


Fig. 2: 100-s binned, background-subtracted X-ray light curve of 4FGL J0935.3+0901 in 0.3–10 keV. The same light curve of the comparison source is also shown. For clarity, the latter light curve is upshifted by 0.2 cts s^{-1} .

To extract photons of J0935.3+0901 and the comparison source, a circular region with radius $24''$ was respectively used. The same-size background regions, local to the two sources respectively, were used. The best-quality data with $\text{FLAG}=0$ and $\text{PATTERN} \leq 4$ for pn and $\text{PATTERN} \leq 12$ for MOS1/MOS2, plus $\#\text{XMMEA_EP}$ and $\#\text{XMMEA_EM}$ (for pn and MOS1/MOS2, respectively), were selected and used. For variability analysis, we used the SAS tasks `evselect` and `epiclccorr` to extract light curve data of the two sources. The final light curves were background-subtracted, produced by combining the data of MOS1, MOS2, and pn.

We also obtained an EPIC spectrum of J0935.3+0901, combined from MOS1, MOS2, and pn data using `epicspeccombine`. Each spectral bin contains at least 20 counts.

2.2 FAST Observation

We observed 4FGL J0935.3+0901 with FAST (Nan 2006) on 2020 August 23, lasting 20 min from 12:35:00 to 12:55:00 (UTC). The Pulsar Backend system was used, which has 4096 channels in the waveband of 1.05–1.45 GHz. A sampling of $49.152 \mu\text{s}$ was chosen in order to detect millisecond pulsation signals. The observation was conducted with the telescope in the tracking mode.

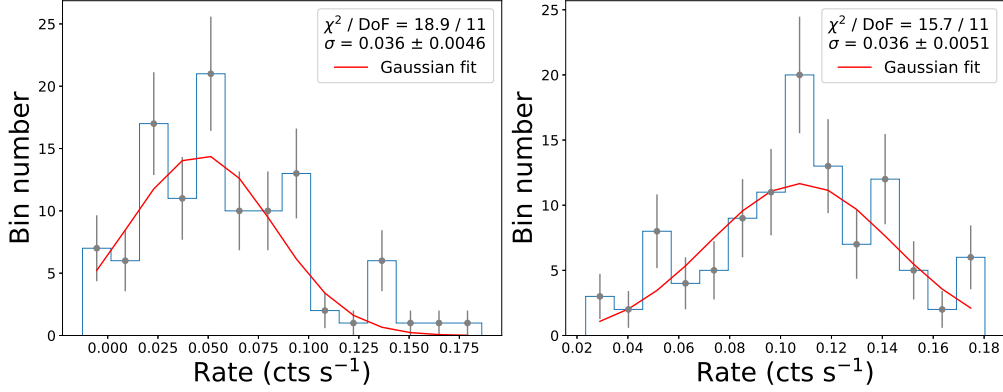


Fig. 3: Count-rate distributions for 4FGL J0935.3+0901 (*left*) and the comparison source (*right*), constructed from the 100-s binned light curves. The best-fit Gaussian functions to each distributions are shown as red curves.

The periodicity searching was performed with the pulsar processing software PRESTO (Ransom 2001; Ransom et al. 2002, 2003). The dispersion measure (DM) from the Earth to 4FGL J0935.3+0901 is likely in a range of from 15.00 to 28.31 pc cm^{-3} , suggested by the estimated distance range for the source (0.76–2.4 kpc; see below Section 4) based on the YMW16 electron-density model (Yao et al. 2017). The time series were dedispersed over DMs in the likely range using a DM step of 0.1 pc cm^{-3} . We applied the acceleration search to retain sensitivity for possible binary pulsar by setting the `zmax` value to be 300, and folded the dedispersed time series on the candidate signals identified by the `ACCEL_sift` subroutine. No convincing pulsation signals were detected.

3 RESULT

3.1 X-ray variability

A distinctive feature of the tMSPs in the disk state is their bimodal distribution of X-ray count rates with fast (as short as tens of seconds) switching timescales between the two count-rate levels (e.g., Patruno et al. 2014). While the faintness of the source hampered our analysis to some degree, we did not see such a feature in J0935.3+0901. In Figure 2, a light curve binned in 100 s in 0.3–10 keV is shown as an example. No phenomenon that the count rates stay at a high level most time and can jump to a ~ 10 times lower level in 10–100 s (see Patruno et al. 2014; Bogdanov & Halpern 2015; Coti Zelati et al. 2019) is seen. We tested different time bins, such as 10 s and 50 s, but the results were nearly the same. Therefore neither two count-rate levels nor fast switching are evident in X-ray emission of the source.

We constructed the count-rate distribution from the 100-s binned light curve of J0935.3+0901, which is shown in Figure 3. To study any possible differences between it and that of the comparison source, which would help identify any possible variability of the target, the same distribution of the comparison source was also constructed. It can be seen that the comparison source was brighter, with the distribution peak value μ at $\sim 0.11 \text{ cts s}^{-1}$. The value for J0935.3+0901 is at $\sim 0.05 \text{ cts s}^{-1}$. We used a Gaussian function,

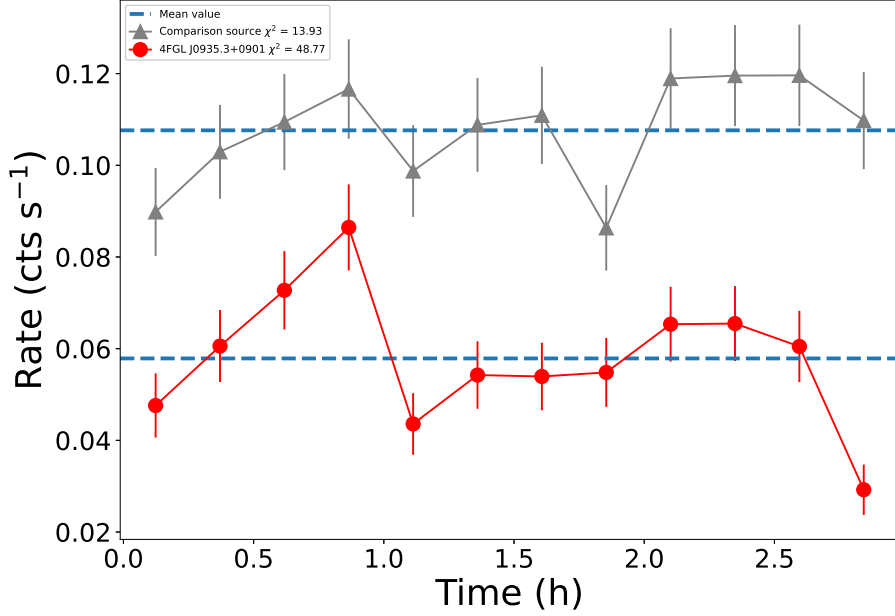


Fig. 4: 890-s binned, background-subtracted light curves of 4FGL J0935.3+0901 (red) and the comparison source (grey).

$\sim \exp[-(x-\mu)^2/2\sigma_g]$, to fit the two distributions, and obtained $\sigma_g \simeq 0.036 \pm 0.005$ for both J0935.3+0901 and the comparison source. The χ^2 values were 18.9 and 15.7 respectively (with 11 degrees of freedom). From the fitting, it can be seen that the distributions can generally be described with a Gaussian function. For J0935.3+0901, a couple of data points, for example the one at $\sim 0.14 \text{ cts s}^{-1}$, are notably away from the best-fit Gaussian function, which is reflected from the slightly larger χ^2 value. However, the deviations are not significant. We thus conclude that the two sources have similar count-rate distributions.

Because J0935.3+0901 is a 2.5-hr binary, determined from optical photometry, we also checked its relatively long time-duration variations. A 890-s binned light curve, containing 12 data points, was constructed (Figure 4). We fit the light curve with a constant, and the resulting χ^2 value was 48.77 (11 degrees of freedom). The same analysis was conducted for the comparison source, and the χ^2 value was 13.93. The X-ray emission of J0935.3+0901 was seemingly variable, by comparing with that of the comparison source. However the light curves of the two sources appear to have a similar temporal pattern. Their correlation coefficient was found to be ~ 0.3 , suggesting weak correlation. We checked our data analysis for possible background contamination, but no such effects were found. Therefore we conclude that possible orbital variations were seen in the target.

3.2 X-ray Spectrum

The 0.3–10 keV spectrum of J0935.3+0901, combined from MOS and pn data, is shown in Figure 5. The spectrum can be well fit with an absorbed power law. Using XSPEC (version 12.10.1f) for the fitting, we obtained a photon index of $1.88_{-0.22}^{+0.25}$ and hydrogen column density $7.2_{-4.5}^{+5.2} \times 10^{20} \text{ cm}^{-2}$, where the errors

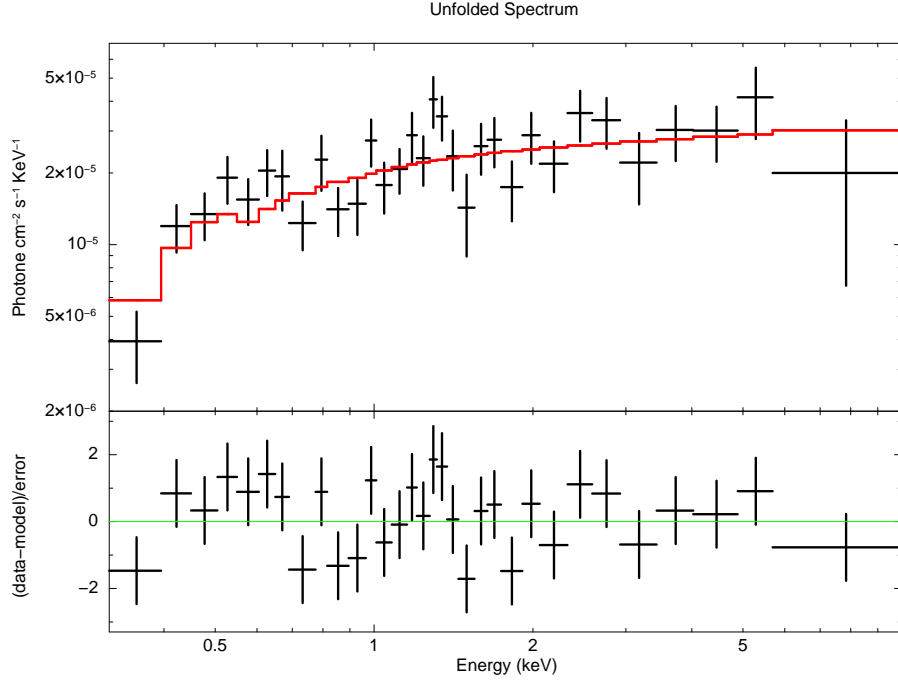


Fig. 5: X-ray spectrum of 4FGL J0935.3+0901 in 0.3–10 keV. The spectrum can be well fit with an absorbed power law (red curve).

are at a 90% confidence level (the reduced χ^2 is 1.15 for 29 degrees of freedom). The resulting 0.3–10 keV absorbed flux is $1.23^{+0.09}_{-0.11} \times 10^{-13} \text{ erg s}^{-1} \text{ cm}^{-2}$, and the unabsorbed is $1.45 \pm 0.15 \times 10^{-13} \text{ erg s}^{-1} \text{ cm}^{-2}$. We note that the Galactic hydrogen column density value (HI4PI Collaboration et al. 2016) is slightly lower than that we obtained, but within the uncertainty.

3.3 FAST upper limit

Because no pulsation signals were detected in our FAST observation, we derived a flux density upper limit from the observation. The modified radiometer equation (Dewey et al. 1985; Patruno et al. 2017)

$$S_{min} = \frac{(S/N)\beta(T_{sys} + T_{sky})}{G\sqrt{n_p t_{obs} \Delta\nu}} \sqrt{\frac{W}{P - W}}, \quad (1)$$

was used, where the correction factor β was assumed to be 1, the number of polarizations n_p was 2, the observation time t_{obs} was 20-min, and the bandwidth $\Delta\nu \simeq 400 \text{ MHz}$. Considering the fundamental performance of FAST described in Jiang et al. (2020), we adopted 20 K for $T_{sys} + T_{sky}$ and 16 K Jy^{-1} for G , where T_{sys} is the system noise temperature, T_{sky} the sky temperature, and G the gain of the telescope. Assuming a pulse duty cycle of 10% (W and P are the effective pulse width and the pulse period respectively), the upper limit value obtained was $0.4 \mu\text{Jy}$ when $S/N = 1$. Thus the upper limit on the flux density of 4FGL J0935.3+0901 was $\sim 4 \mu\text{Jy}$ (when requiring $S/N=10$).

4 DISCUSSION

We have observed 4FGL J0935.3+0901 with *XMM-Newton* for the purpose of further identifying its nature, whether it could be a candidate tMSP in the sub-luminous disk state. From X-ray variability analysis, we did not find evidence for a bimodal count-rate distribution, which would be expected from a tMSP in the disk state. The *XMM-Newton* observation confirmed the faintness of the source at X-rays, as the obtained unabsorbed flux was $1.45 \times 10^{-13} \text{ erg s}^{-1} \text{ cm}^{-2}$, similar to the face value of the X-ray flux obtained from short *Swift* observations reported in Wang et al. (2020). The X-ray-to- γ -ray flux ratio now is updated to be 0.030 ± 0.007 . Both the variability analysis results and the flux ratio value indicate that the source is not a tMSP in the disk state; instead the both, plus the X-ray photon index as well (the indices of redbacks are generally in a range of 1–2), are consistent with the properties of redbacks in the pulsar state (Miller et al. 2020).

We found that the source’s X-ray emission was possibly variable, while it is hard to determine whether the variability was related to the 2.5-hr orbit because of the limited observation time ($\simeq 3$ hrs). Many redbacks in the pulsar state were found to be X-ray variable. They can show clear orbital modulation (e.g., Bogdanov et al. 2011; Linares 2018), flaring-like variations (e.g., Halpern et al. 2017; Cho et al. 2018), or weak variations possibly related to binary orbits (e.g., Li et al. 2016, 2018). The X-ray variations likely reflect intrabinary physical processes related to the pulsar winds, such as the intrabinary shock (Bogdanov et al. 2011) or magnetic reconnection in a striped pulsar wind (Al Noori et al. 2018). In this respect, the possible X-ray variation of J0935.3+0901 fits in the properties of redbacks. According to X-ray studies of redbacks, their X-ray luminosities in the pulsar state are lower than $10^{32} \text{ erg s}^{-1}$ (Linares 2014) and can be as low as $\sim 10^{31} \text{ erg s}^{-1}$ (Strader et al. 2019). This would put J0935.3+0901 at a distance of 0.76 kpc ($(L_X/10^{31} \text{ erg s}^{-1})^{1/2}$), or $\leq 2.4 \text{ kpc}$ when requiring its X-ray luminosity $\leq 10^{32} \text{ erg s}^{-1}$.

Considering 4FGL J0935.3+0901 as a redback in the disk-free, pulsar state, an explanation is needed for the double-peaked emission lines present in its optical emission, as such features are typically seen in spectra of accretion disks around compact stars. The other possibility of arising from an outflow from the companion and/or the intrabinary shock region (see Swihart et al. 2018 and references therein) should be the case. The emission features of J0935.3+0901 would be highly variable, which can be verified by spectroscopic observations. The existence of the intrabinary material could block the radio pulsed emission, i.e., the often-seen eclipsing phenomenon in compact MSP binaries, and thus we did not detect the signals at the deep sensitivity level of $\sim 4 \mu\text{Jy}$ with FAST. Hopefully in the near future, further effort through multi-wavelength observations, including a radio observation covering the whole binary orbit (in order to avoid possible eclipsing phases), may finally be able to provide a clear picture for this source.

Acknowledgements This research is supported by the National Natural Science Foundation of China (11633007) and the Original Innovation Program of the Chinese Academy of Sciences (E085021002). J.V. thanks Prof. C.D. Ravikumar for the support and timely help.

References

- Abdollahi, S., Acero, F., Ackermann, M., et al. 2020, *ApJS*, 247, 33
- Al Noori, H., Roberts, M. S. E., Torres, R. A., et al. 2018, *ApJ*, 861, 89
- Archibald, A. M., Stairs, I. H., Ransom, S. M., et al. 2009, *Science*, 324, 1411
- Bassa, C. G., Patruno, A., Hessels, J. W. T., et al. 2014, *MNRAS*, 441, 1825
- Benvenuto, O. G., De Vito, M. A., & Horvath, J. E. 2014, *ApJ*, 786, L7
- Bhattacharya, D., & van den Heuvel, E. P. J. 1991, *Phys. Rep.*, 203, 1
- Bogdanov, S., Archibald, A. M., Hessels, J. W. T., et al. 2011, *ApJ*, 742, 97
- Bogdanov, S., & Halpern, J. P. 2015, *ApJ*, 803, L27
- Chen, H.-L., Chen, X., Tauris, T. M., & Han, Z. 2013, *ApJ*, 775, 27
- Cho, P. B., Halpern, J. P., & Bogdanov, S. 2018, *ApJ*, 866, 71
- Coti Zelati, F., Papitto, A., de Martino, D., et al. 2019, *A&A*, 622, A211
- Dewey, R. J., Taylor, J. H., Weisberg, J. M., & Stokes, G. H. 1985, *ApJ*, 294, L25
- Halpern, J. P., Bogdanov, S., & Thorstensen, J. R. 2017, *ApJ*, 838, 124
- He, L., et al. 2019, *Research in Astronomy and Astrophysics*, 19, 098
- HI4PI Collaboration, Ben Bekhti, N., Flöer, L., et al. 2016, *A&A*, 594, A116
- Jiang, P., Tang, N.-Y., Hou, L.-G., et al. 2020, *Research in Astronomy and Astrophysics*, 20, 064
- Li, K.-L., Kong, A. K. H., Hou, X., et al. 2016, *ApJ*, 833, 143
- Li, K.-L., Hou, X., Strader, J., et al. 2018, *ApJ*, 863, 194
- Linares, M. 2014, *ApJ*, 795, 72
- Linares, M. 2018, *MNRAS*, 473, L50
- Miller, J. M., Swihart, S. J., Strader, J., et al. 2020, *ApJ*, 904, 49
- Nan, R. 2006, *Science in China: Physics, Mechanics and Astronomy*, 49, 129
- Patruno, A., Archibald, A. M., Hessels, J. W. T., et al. 2014, *ApJ*, 781, L3
- Patruno, A., Jaodand, A., Kuiper, L., et al. 2017, *ApJ*, 841, 98
- Ransom, S. M. 2001, *New search techniques for binary pulsars*, PhD thesis, Harvard University
- Ransom, S. M., Cordes, J. M., & Eikenberry, S. S. 2003, *ApJ*, 589, 911
- Ransom, S. M., Eikenberry, S. S., & Middleditch, J. 2002, *AJ*, 124, 1788
- Roberts, M. S. E. 2013, in *Neutron Stars and Pulsars: Challenges and Opportunities after 80 years*, ed. J. van Leeuwen, Vol. 291, 127
- Shahbaz, T., Linares, M., Nevado, S. P., et al. 2015, *MNRAS*, 453, 3461
- Stappers, B. W., Archibald, A. M., Hessels, J. W. T., et al. 2014, *ApJ*, 790, 39
- Strader, J., Swihart, S., Chomiuk, L., et al. 2019, *ApJ*, 872, 42
- Swihart, S. J., Strader, J., Shishkovsky, L., et al. 2018, *ApJ*, 866, 83
- Takata, J., Li, K. L., Leung, G. C. K., et al. 2014, *ApJ*, 785, 131
- Wang, Z., Xing, Y., Zhang, J., et al. 2020, *MNRAS*, 493, 4845

Yao, J. M., Manchester, R. N., & Wang, N. 2017, ApJ, 835, 29